

NADPH and NAC synergistically inhibits chronic ocular hypertension-induced neurodegeneration and neuroinflammation through regulating p38/MAPK pathway and peroxidation

Naiji Yu ^{a,1}, Xingdi Wu ^{a,1}, Chengshou Zhang ^{a,1}, Qiyu Qin ^a, Yuxiang Gu ^b, Weishaer Ke ^c, Xin Liu ^a, Qi Zhang ^a, Zhenjie Liu ^{d,*}, Min Chen ^{a,*}, Kaijun Wang ^{a,*}

^a Eye Center, The Second Affiliated Hospital, School of Medicine, Zhejiang University, Zhejiang Provincial Key Laboratory of Ophthalmology, Zhejiang Provincial Clinical Research Center for Eye Diseases, Zhejiang Provincial Engineering Institute on Eye Diseases, Hangzhou, Zhejiang 310000, China

^b Department of Ophthalmology, The First People's Hospital of Xiaoshan District, Xiaoshan Affiliated Hospital of Wenzhou Medical University, Hangzhou, Zhejiang 311200, China

^c Department of Ophthalmology, Xinjiang 474 Hospital, Urumqi, Xinjiang 841100, China

^d Department of Vascular Surgery, The Second Affiliated Hospital, School of Medicine, Zhejiang University, Hangzhou, Zhejiang 310000, China

ARTICLE INFO

Keywords:

Ocular hypertension
Retinal ganglion cell
Müller cell
Antioxidants
MAPK

ABSTRACT

Glaucoma, the leading cause of irreversible blindness worldwide, is characterized by neurodegeneration and neuroinflammation with retinal NAD/NADP and GSH decline. Nicotinamide adenine dinucleotide (NAD)/NAD phosphate (NADP) and glutathione (GSH) are two redox reducers in neuronal and glial metabolism. However, therapeutic strategies targeting NAD/NADP or GSH do not exert ideal effects, and the underlying mechanisms are still poorly understood. We assessed morphological changes in retinal ganglion cells (RGCs), the affected neurons in glaucoma, and Müller cells, the major glial cells in the retina, as well as the levels of phosphorylated p38 (p-p38) and Caspase-3 in glaucoma patients. We constructed a modified chronic ocular hypertensive rat model and an oxygen-glucose deprivation (OGD) cell model. After applying NADPH and N-acetylcysteine (NAC), a precursor to cysteine, the rate-limiting substrate in GSH biosynthesis, to cells, apoptosis, axonal damage and peroxidation were reduced in the RGCs of the NAC group and p-p38 levels were decreased in the RGCs of the NADPH group, while in stimulated Müller cells cultured individually or cocultured with RGCs, gliosis and p38/MAPK, rather than JNK/MAPK, activation were inhibited. The results were more synergistic in the rat model, where either NADPH or NAC showed crossover effects on inhibiting peroxidation and p38/MAPK pathway activation. Moreover, the combination of NADPH and NAC ameliorated RGC electrophysiological function and prevented Müller cell gliosis to the greatest extent. These data illustrated conjoined mechanisms in glaucomatous RGC injury and Müller cell gliosis and suggested that NADPH and NAC collaborate as a neuroprotective and anti-inflammatory combination treatment for glaucoma and other underlying human neurodegenerative diseases.

1. Introduction

Glaucoma is manifested by the apoptosis and other forms of programmed cell death of retinal ganglion cells (RGCs) and the loss of their axons [1]. As a retinal neurodegenerative disease, glaucoma has a complex pathogenesis. In addition to elevated intraocular pressure (IOP), a variety of other factors have been shown to play primary roles, including elevated glutamate levels, altered nitric oxide (NO) metabolism, vascular changes and oxidative stress damage associated with

reactive oxygen species (ROS) [2].

Abnormally elevated ROS levels can lead to cell apoptosis, necrosis, ferroptosis, or other damage through the oxidation of macromolecules such as proteins, lipids, nuclear DNA, or mitochondrial DNA [3–6]. ROS accumulation is also related to mitogen-activated protein kinase (MAPK) signaling activation, which is involved in cell proliferation, cell differentiation, cell stress and inflammation [7]. In recent years, elevated ROS levels have been recognized as an important mechanism of cell death in neurodegenerative diseases, including glaucoma [8]. An

* Corresponding authors.

E-mail addresses: lawson4001@zju.edu.cn (Z. Liu), chenmineye@zju.edu.cn (M. Chen), ze_wkj@zju.edu.cn (K. Wang).

¹ Contributed equally.

increase in ROS levels leads to mitochondrial dysfunction and further alterations in neurodegenerative markers [9], which can cause preferential degeneration of specific subtypes of RGCs during energy production [10]. Studies on ROS scavenger medication have illustrated their underlying utility in glaucoma treatment [8,11,12]. In addition, levels of ROS are associated with risk factors such as increased IOP and age, which may explain the underlying peroxidative effects of glaucoma development [13].

There are two independent antioxidative systems in eukaryotic organisms, the thioredoxin (TXN) system and the glutathione (GSH) system [14]. Efficient running of the two antioxidative systems maintains the redox level and inhibiting both of them triggers cell death [15]. Notably, both systems must be inhibited to trigger cell death, since one system may compensate another [16]. A decrease in the levels of two pivotal molecules in the antioxidative systems, nicotinamide adenine dinucleotide (NAD)/NAD phosphate (NADP) and GSH, has been found in glaucomatous retinas [17,18]. Cysteine is the rate-limiting substrate in GSH biosynthesis and is largely generated via GSH- or thioredoxin reductase 1 (TXNRD1)-mediated reduction [19]. Reduced NADP (NADPH) plays a core antioxidant role not only in mevalonate biosynthesis and the de novo synthesis and elongation of fatty acids but also in the GSH- and TXN-dependent systems [20]. Although the therapeutic effects of cysteine and NADPH in a variety of neurodegenerative diseases have been studied, the impact of cysteine and NADPH on glaucomatous neurodegeneration and neuroinflammation remains to be elucidated [21]. In addition, their effects on MAPK signaling are also undefined.

We have mentioned that MAPK signaling modulates cell proliferation and differentiation, and previous studies have shown that abnormal interactions between retinal glial cells (Müller cells, astrocytes and microglia) and RGCs also play a key role in the pathogenesis of glaucoma [22,23]. Müller cells, the main glial cells in the retina, support the functional metabolism of neurons and regulate retinal vascular permeability, including recycling neurotransmitters through their transporters and maintaining retinal K⁺ and water homeostasis via various K⁺ and Ca²⁺ channels [24]. Müller cell gliosis protects neuronal survival through the synthesis of neurotrophins and antioxidants [24], but the release of toxic cytokines and intake dysfunction-induced overload of glutamate damage RGCs in the long run [23,25,26]. Nevertheless, few studies have explored how cysteine and NADPH regulate Müller cell gliosis and its neuronal effects.

We established chronic glaucoma models and focused on how NAC, a precursor to cysteine, and NADPH affected the p38/MAPK signaling pathway in RGCs and Müller cells. We revealed the linked mechanisms of p38/MAPK activation and peroxidation in glaucomatous RGC apoptosis and Müller cell gliosis for the first time, and the clinical value of NAC and NADPH on glaucomatous RGC damage and Müller cell gliosis via these linked mechanisms was further proven.

2. Methods

2.1. Human eye tissue

Human retinas were collected from 3 patients with end-stage glaucoma and 3 deceased healthy donors after eye enucleation (Table S1). A triangle-shaped retina flat with its vertex pointing to posterior pole and its base locating 1 cm from optic nerve was collected from every sample. Retinas were routinely fixed, dehydrated, embedded, and sectioned (5 µm) for later analysis of HE staining, immunofluorescent/ immunohistochemical staining or transmission electron microscopy (TEM). All human retinal tissues were obtained from the Eye Center, The Second Affiliated Hospital, School of Medicine, Zhejiang University between February 2021 and September 2021. Acquisitions and experiments involving human tissue were performed in accordance with The Code of Ethics of the World Medical Association (Declaration of Helsinki) and were approved by the Human Research Ethics Committee of the Second Affiliated Hospital, School of Medicine, Zhejiang University (No.

120211118).

2.2. Animals

Male SD rats weighing 200–250 g were purchased from Vital River Laboratory Animal Technology Co., Ltd (Beijing, PRC) and housed in illumination (12: 12 h light: dark cycle) and temperature-controlled and pathogen-free facilities with free access to clean water and food. All animal care and experiments were approved by the Laboratory Animal Ethics Committee of the Second Affiliated Hospital, School of Medicine, Zhejiang University (No.2023–004) and conducted in accordance with the Association for Research in Vision and Ophthalmology Statement for the Use of Animals in Ophthalmic and Vision Research.

2.3. Purification of primary RGCs

Primary RGCs were purified and cultured in accordance with our previous study [27]. Briefly, the retina isolated from P7 mice (C57BL/6, purchased from the Charles River Laboratories) was dissected under a microscope and digested to single-cell by papain. For purification, the cell suspension was processed through three-step panning: (i) incubation in a negative panning plate coated by the lectin for 30 min (shake the dish gently per 15 min); (ii) incubation in another lectin-coated dish for 10 min; (iii) incubation in a positive panning plate coated with anti-mouse-Thy1.2 antibody (Bio-Rad Laboratories, USA) for 45 min (shake the dish per 15 min). Cells attached to the plate were digested with trypsin and collected. After resuspension, purified RGCs were seeded on glass coverslips coated with mouse Laminin (R&D Systems, USA) and Poly-D-Lysine (Sigma-Aldrich, USA) and cultured by RGC growth medium (equivalent Neurobasal Medium and DMEM containing supplemental factors). We maintained RGCs in a humidified incubator containing 5 % CO₂ and 95 % air at 37 °C and performed following interventions 2 days later.

2.4. Rat model of chronic ocular hypertension

Polystyrene beads (Polysciences, USA) were adequately shaken, dropped out and centrifuged at 2000 rpm for 1 min. After removing the supernatant, a sufficient volume of 75 % ethanol was added for vortexing, and then the mixture was centrifuged and repeatedly washed 2 times. The 6 µm and 10 µm diameter beads were dispersed in normal saline (NS) containing 0.1 % carbomer (molecular weight 4 mDa) at a concentration of 1 × 10⁷/mL. Before injection, 5 µL of 6 µm diameter beads, 5 µL of 10 µm diameter beads, and 2 µL of air were taken up into a microsyringe (Hamilton, Switzerland) through a 33-gauge needle in turn.

After general anesthesia (1 % sodium pentobarbital, 5 mL/kg), proparacaine eye drops (Alcon, USA) were applied for local anesthesia. Normal sterilization and anterior chamber (AC) paracentesis were conducted with a 32-gauge needle before the microbeads were quickly injected into the central AC with the prepared microsyringe through the canal. Finally, the bubbles were adjusted to the inner mouth of the canal, and the needle was withdrawn 1 min later. Levofloxacin eye drops (Santen, Japan) were applied for disinfection. TonoLab (Icare, Finland) was used as an IOP monitor without anesthesia. The microbead injection was repeated under nonideal IOP elevation at Day 7. Eyes with endophthalmitis, intraocular bleeding, corneal perforation, or obvious anterior chamber leakage were excluded.

2.5. Oxygen/glucose deprivation (OGD)

For Müller cells (MIO-M1 cell line), 0.3 g/L glucose was formulated with glucose and DMEM (glucose free, Thermo Fisher Scientific, USA), and applied to Müller cells in a 0.5 % O₂, 5 % CO₂ atmosphere for 22 h. For RGCs or Müller cell-RGC co-cultured system, 0.3 g/L glucose was formulated with RGC growth medium and DMEM, and cultured in a 0.5

% O₂, 5 % CO₂ atmosphere for 4 h. Cells were incubated with fluorescent probes for living image or changed into the environment with proper glucose concentration and atmosphere for Transwell or scratch wounding assays. The cell line was tested to be free of mycoplasma contamination and was authenticated via STR profiling.

2.6. Live/dead assay

Using Viability/Cytotoxicity Assay Kit (US EVERBRIGHT, PRC), cells were gently washed with PBS once and stained with Calcein AM (2 μM) and Ethidium homodimer-1 (EthD-1, 4 μM) for 15 min at 37 °C. Finally, the images of live (green) and dead (red) cells were observed under a fluorescence microscope (Leica DMI8, Germany).

2.7. ROS measurement

ROS was detected with dihydroethidium (DHE) (Beyotime, PRC). RGCs were loaded with 5 mM DHE for 30 min at 37 °C while frozen sections were loaded with 200 mM DHE for 30 min at room temperature (RT) following 3 times PBS wash and DAPI Fluoromount-G™ (Yeasen Biotech, PRC) staining. RGCs or sections were observed under a fluorescence microscope (Leica DMI8 for RGCs or DM6B for sections).

2.8. Scratch wounding migration

Müller cells were seeded in a 6-well plate at a density of 5×10^5 cells/well in 2 mL of medium overnight. The confluent cell monolayers were scratched by a sterile 200-μL micropipette tip and washed with PBS. After OGD, the medium was changed to a complete medium without NAC or NADPH. Cell migration was examined using a light microscope (Leica DMI1) at scratching or 24 h after OGD, and the scratch widths were quantified by ImageJ software (NIH, USA).

2.9. Transwell assay

The second day of RGC purification, Müller cells (1×10^4) were seeded on an 8 μm pore diameter-Transwell and cultured overnight upon RGCs (inner Transwell, 100 mL, outer Transwell, 300 mL). After OGD, supernatants from RGCs were half removed, resulting in 150 mL remaining, and 150 mL DMEM with extra glucose was added to outer Transwell forming a 1 g/L glucose concentration. Inner Transwell was treated similarly to build a 1 g/L glucose concentration. Additionally, 3 μL fetal bovine serum (FBS) was pipetted to outer Transwell in order to accelerate the migration process. Migration after OGD lasts 24 h under 5 % CO₂ and 95 % air. Furthermore, Müller cells without pre-OGD treatment were treated by supernatants from 6 h re-oxygenated RGCs and performed this migration exam again. Müller cells were fixed with 4 % paraformaldehyde (PFA) for 15 min washed with PBS and stained with crystal violet (Beyotime). Cells inner Transwell were abraded with cotton swabs and migrated cells were imaged by a Leica DMI1 light microscope. Cells were quantified by ImageJ software.

2.10. Rat eyeballs processing for morphological examination

After being sacrificed, eyes or optic nerves were enucleated under a stereomicroscope (Leica S9i) and fixed with 4 % PFA following eradication of cornea, iris, lens and extraocular muscle tissue reserving posterior segments (eye cups). For the paraffin section, eye cups or optic nerves were normal dehydration (Leica ASP300S) and paraffin embedded. 5-μm thickness paraffin sections were cut parallel with the optic axis through the optic disks or traverse optic nerves 1 mm from eyeballs. Sections were stained with hematoxylin and eosin (H&E) or dewaxed, rehydrated and boiling citrate buffer incubated for antigen retrieval. For the frozen section, eye cups were dehydrated in 5 %, 12.5 % and 20 % sucrose (m/v, in PBS) and embedded in an equivalent OCT compound and 20 % sucrose. 8-μm thickness frozen sections were cut

paralleled with the optic axis through the optic disks and used for staining immediately. For retinal mounts, retinas were gently torn against sclera tissues and cut into four-leaf clovers unfolding on slides. Then cold methanol was dropped for degreasing and flat mounts were immersed and reserved in methanol at -20 °C.

In the H&E-stained section, 4 standard areas of each sample were used for cell quantification in RGCL. Every standard area contained a 200 μm-length retina which was located at 1 mm from the optic disk and 2 researchers blind to rat grouping calculated the cell number in RGCL independently.

In retinal flat mount, fluorescent signal was imaged once every 0.5 μm step on z-stack, 3D structure reconstruction and signal colocalization were conducted with Imaris 9.0.1 (Oxford Instrument, UK) and MATLAB Compiler Runtime V8.4 (Mathworks, USA).

2.11. Immunohistochemistry (IHC)

After deparaffinization and antigen retrieval, sections were washed with PBS once and immersed in 3 % H₂O₂ for 10 min at RT and blocked with normal goat serum (NGS) for 1 h at RT. Thereafter, sections were incubated at 4 °C overnight with the following primary antibodies. Sections were then washed with PBS and incubated with horseradish peroxidase (HRP)-conjugated goat anti-rabbit IgG polyclonal antibodies for 23 min at RT. The sections were stained with 3,3'-diaminobenzidine and counterstained with hematoxylin. Then, sections were washed with water and mounted in neutral balsam. All slides were imaged with a light microscope (Leica DM2500) and uncalibrated optical density (OD) was calculated with ImageJ software.

2.12. Immunofluorescent (IF) staining

The frozen sections or RGCs cultured on coverslips were fixed with 4 % PFA for 10 min and permeabilized with 0.3 % Triton X-100 and 0.2 % bovine serum albumin (BSA) in PBS for 1 h at RT. The retinal mounts and antigen-retrieved paraffin sections were washed with PBS once and permeabilized the same as frozen sections. After rinsed 3 times in PBS, they were blocked in buffer (5 % NGS, 2 % BSA, and 0.1 % Tween-20 in PBS) for 1 h at RT. Then they were incubated with primary antibody (Table S2) at 4 °C overnight and species-specific secondary fluorescent antibodies for 4 h (retina mounts) or 1 h (RGCs and sections) at RT. After being washed with PBS, samples were stained with DAPI and imaged with a Leica DM6B fluorescence microscope or a Leica SP8 confocal microscope.

2.13. TUNEL assay

Terminal transferase deoxyuridine triphosphate nick end labeling (TUNEL) assay was performed using frozen sections according to the manufacturer's methods of One-Step TUNEL Apoptosis Assay Kit (Beyotime, China). Finally, the sections were stained with DAPI and observed under a Leica DMI8 microscope. TUNEL-positive cells were labeled in a standard area same as RGCL cell counting.

2.14. Western blot (WB)

Total protein was extracted by Total Protein Extraction Kits (Solarbio, PRC) with lysis buffer 60 μL/well (6-well plate) or 300 μL/rat retina. Retina should be 270 W ultrasonicated for 2 s twice by ultrasonic disruptor (Scientz, PRC) when lysis buffer was added. Protein concentration was quantified by a Pierce™ BCA Protein Assay Kit (Thermo Fisher Scientific, Massachusetts, USA) and diluted with lysis buffer to equalization and the final resolution was mixed with loading buffer (Sangon Biotech, PRC).

Equal amounts of protein were electrophoresed on 12 % or 4~20 % SDS PAGE Gels (ACE Biotechnology, PRC) and transferred to PVDF membranes (Millipore, USA). Membranes were then blocked with

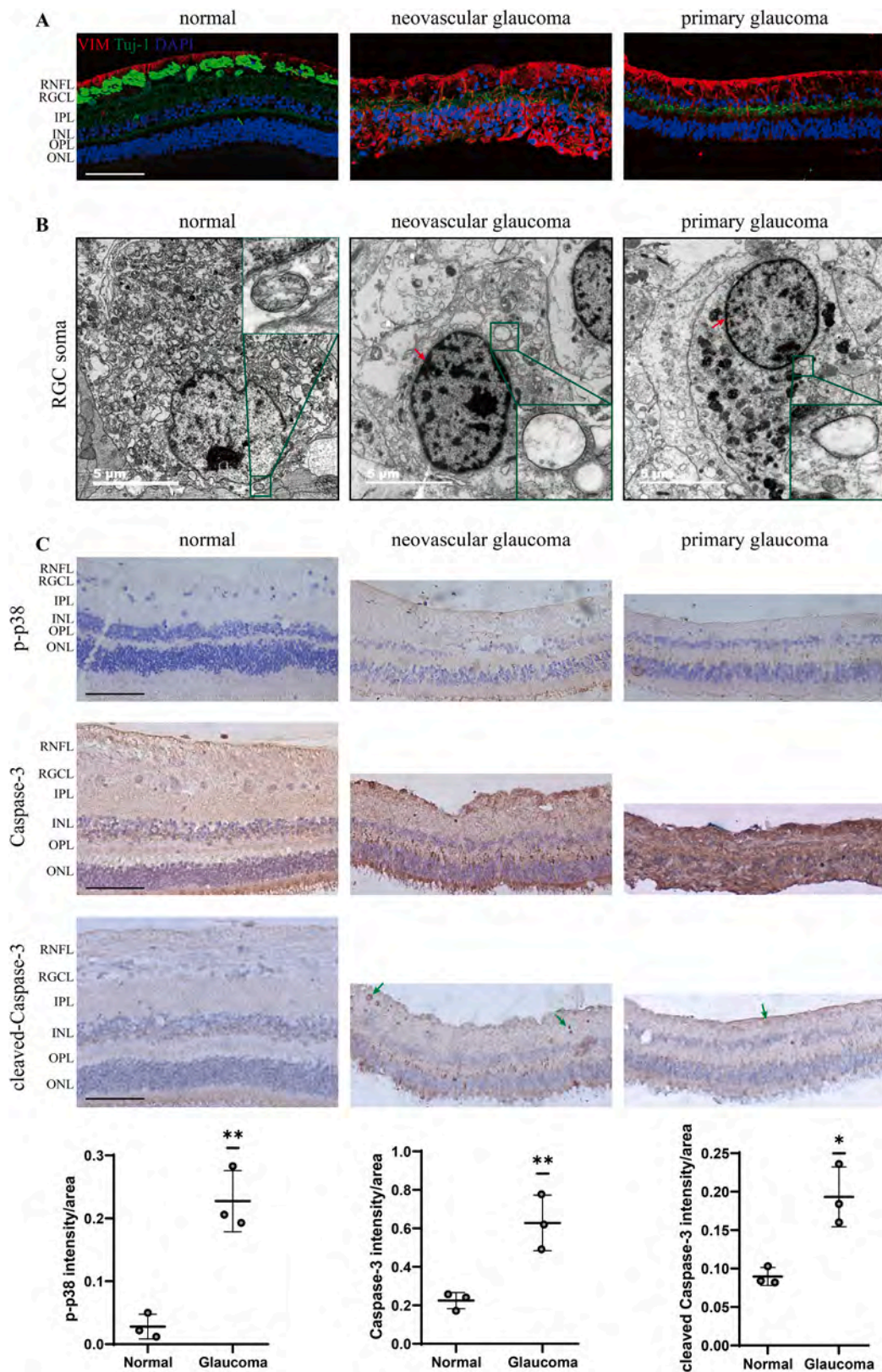
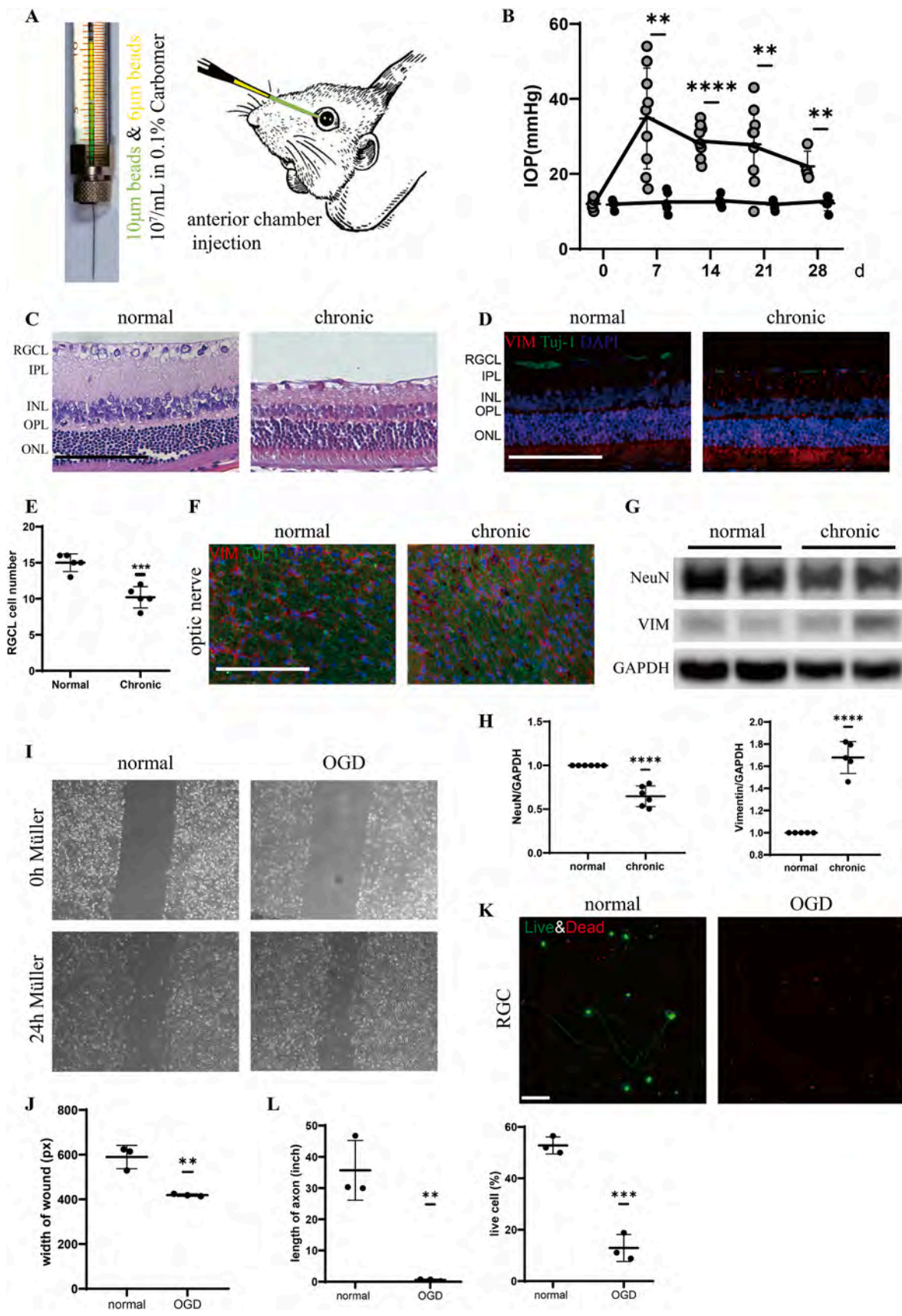


Fig. 1. Morphology of Müller cells, apoptosis of RGCs and expression of p-p38 in glaucomatous retinas. (A) VIM and Tuj-1 IF staining images of retinal sections from a healthy donor, a NVG patient and a primary open-angle glaucoma patient, scale bar = 100 μ m. (B) TEM images of RGCs from corresponding human retinas, scale bar = 5 μ m. (C) p-p38, Caspase-3 and cleaved Caspase-3 IHC images of corresponding human retinas and statistics of average intensity, scale bar = 100 μ m. Red arrows indicated dense chromatin, green arrows pointed cleaved Caspase-3 positive cells and green squares showed the magnified areas. RNFL: retinal nerve fiber layer; RGCL: retinal ganglion cell layer; IPL: inner plexiform layer; INL: inner nuclear layer; OPL: outer plexiform layer; ONL: outer nuclear layer.



(caption on next page)

Fig. 2. Establishment of COH model and OGD model. (A) Liquid and methods used for COH modeling (fluorescein and indocyanine green marked). (B) IOP measurement before and after microbeads AC injection (grey point as experimental rats, black point as control rats). (C) Representative H&E staining images of normal and COH retinal sections and (D) RGCL cell number statistics. (E) VIM and Tuj-1 IF staining of normal and COH retinal sections and (F) optic nerve cross-sections. (G) NeuN and VIM blots (numbers beside: molecular weight; unit: kDa) of normal and COH retinas and (H) statistics of their gray value. (I) Müller cell scratch wound image from same location before and 24 h after OGD and (J) statistical analysis on width of wound at 24 h after OGD. (K) Calcein AM & EthD-I staining of primary RGCs and (L) statistical analysis on length of axons and rate of live cells. RNFL: retinal nerve fiber layer; RGCL: retinal ganglion cell layer; IPL: inner plexiform layer; INL: inner nuclear layer; OPL: outer plexiform layer; ONL: outer nuclear layer. n = 3 or 4 per group. Error bars = SD. Scale bars = 100 μ m. Comparisons were conducted by t-test. **: p < 0.01; ***: p < 0.001; ****: p < 0.0001.

Protein Free Rapid Blocking Buffer (YaMei, China) for 1 h and probed with primary antibodies at 4 °C overnight and secondary antibodies for 1 h at RT. The blots were cut and separated into sections for different antibody probing (Table S2). Protein expression was detected in a chemiluminescence solution (Bio-Rad, USA) by Chemiluminescence imaging system (Bio-Rad) and analyzed via densitometry with ImageLab software. To calculate the relative expression of a specific protein, the nonphosphorylated form or GAPDH served as a reference.

2.15. Transmission electronic microscopy (TEM)

After fixing in 2.5 % glutaraldehyde in a 0.1 M phosphate buffer for 4 h at RT and overnight at 4 °C, retinas or optic nerves were fixed with 1 % OsO₄ and washed with ddH₂O, followed by dehydration with graded alcohol and embedding in acetone, acetone with 33 % epoxy resin, and epoxy resin successively. Ultrathin sections (50 nm) were cut by a Leica UC7 slicer and placed on copper grids, stained with uranyl acetate and lead citrate, and examined under a 120 kV electron microscope (Tecnaï G2 Spirit, FEI, USA).

2.16. Optical coherence tomography (OCT) imaging

After general anesthesia (1 % sodium pentobarbital, 5 mL/kg), tropicamide phenylephrine eye drops (Santen) were applied for pupillary dilation. Carbomer gel was applied to the cornea to prevent dryness. Images were scanned under the ring scan mode centered by the optic nerve head using a Phoenix Micron IV retinal imaging microscope (Phoenix, USA), and 20 images at the same position were averaged to eliminate artifacts. The Phoenix software traced the edge of retinas around the optic nerve head.

2.17. Electroretinography (ERG)

After general anesthesia (1 % sodium pentobarbital, 4 mL/kg) and 10 min light adaption, rats were performed the full-field ERG test under a Ganzfeld Q450C stimulator (Roland, Germany). Recording electrodes were attached to the central cornea, and reference electrodes were placed hypodermically on the central forehead while grounding electrodes were inserted hypodermically into the root of the tail. To evaluate photopic negative response (PhNR), a period of 2000 μ s red light stimulation was performed at 0.4 cd.s/m² against a royal blue background of 25 cd/m² twice and signals were averaged to eliminate artifacts. The curves of PhNR illustrated in this article were drawn with Origin 2019b (OriginLab, USA), and Savitzky-Golay method was applied with setting points of window at 5–10. The PhNR amplitude was noted with the original data and defined as the potential between the trough following the b-wave and the baseline without signal processing [28].

2.18. Formulation and delivery of NAC and NADPH

NAC (A8199, Sigma-Aldrich, USA) and NADPH tetrasodium salt (HY-F0003, MedChemExpress, USA) were preserved under conditions as manufacturers suggested. For in vitro experiments and intravitreal injection, powders were dissolved to 10 mM in NS and diluted with medium (to different concentrations mentioned in the Results part) for OGD or NS (to a concentration of 0.5 mM NAC, 1 mM NADPH and their equivoluminal mixture) for intravitreal injection, following sterilization

by filtration. The entrance of intravitreal injection was 2 mm posterior to the corneoscleral limbus and 5 μ L solution with 1 % fluorescein sodium was gently injected. Facilities and anesthetics/antibiotics of intravitreal injection were same as AC injection and retinal hemorrhage or obvious leakage individuals were excluded. For in vivo intraperitoneal injection, various doses of NAC (300 mg/kg), NADPH (10 mg/kg) and mixture (150 mg/kg NAC & 5 mg/kg NADPH) were dissolved in NS just before injection according to body weight.

2.19. Statistics

All data were reported as mean \pm standard deviation (SD) and all statistical tests were two-tailed. Results of p < 0.05 were considered statistically significant. All experiments were carried out at least three times. The repeated times of the experiments were given in corresponding captions. Comparisons between 2 groups were analyzed by Student's t-test while multiple groups were assessed by one-way analysis of variance (ANOVA) followed by Bonferroni post hoc test.

3. Results

3.1. Retinal Müller cell gliosis, RGC apoptosis and p38 activation in end-stage glaucoma

The morphology and distribution of retinal Müller cells substantially varied between the healthy donor, primary glaucoma patient and secondary glaucoma patient (Fig. 1A). The total number of Müller cells in normal humans is low, and these cells lack typical outgrowth. Vimentin (VIM) is mainly distributed in the nerve fiber layer. The total number of Müller cells in glaucoma patients significantly increased, and there were many large "amoeba-like" protrusions from the retinal nerve fiber layer (RNFL) to the inner plexiform layer (IPL), especially in the retina from the neovascular glaucoma (NVG) patient that had serious structural damage and almost full layer distribution. In addition, the RGCs within the patients' retina almost completely disappeared, resulting in the retinal ganglion cell layer (RGCL) being difficult to identify, accompanied by thinning of the IPL and whole retina.

TEM images of the above three samples showed that normal retinal RGCs had a complete biomembrane system, while the biomembrane structure of the RGCs in the retina tissue from the NVG patient was ruptured or distorted. In addition, the mitochondria and other organelles of the RGCs from the healthy donor had standard morphology and crest and a complete cytoskeleton, while diseased RGCs lost their structural integrity and showed abnormal morphology such as swelling or vacuolar degeneration (Fig. 1B). The overall density of healthy RGC nuclei was relatively loose, while there was uneven chromatin density and condensed chromatin against nuclear envelopes in the RGCs from the two glaucoma patients, illustrating morphological characteristics of apoptosis.

IHC of the above three samples showed that the expression of Caspase-3, cleaved Caspase-3 and p-p38 in the diseased retinas was higher than that in the healthy retinas (Fig. 1C). In the diseased retinas, p-p38 levels were significantly elevated in the original RGC area and in some cells in the IPL and inner nuclear layer (INL). The expression of Caspase-3 in the original RGC area was significantly upregulated, suggesting that apoptosis had an important impact on RGC loss in the retinas of the two patients. In addition, Caspase-3 levels were increased to

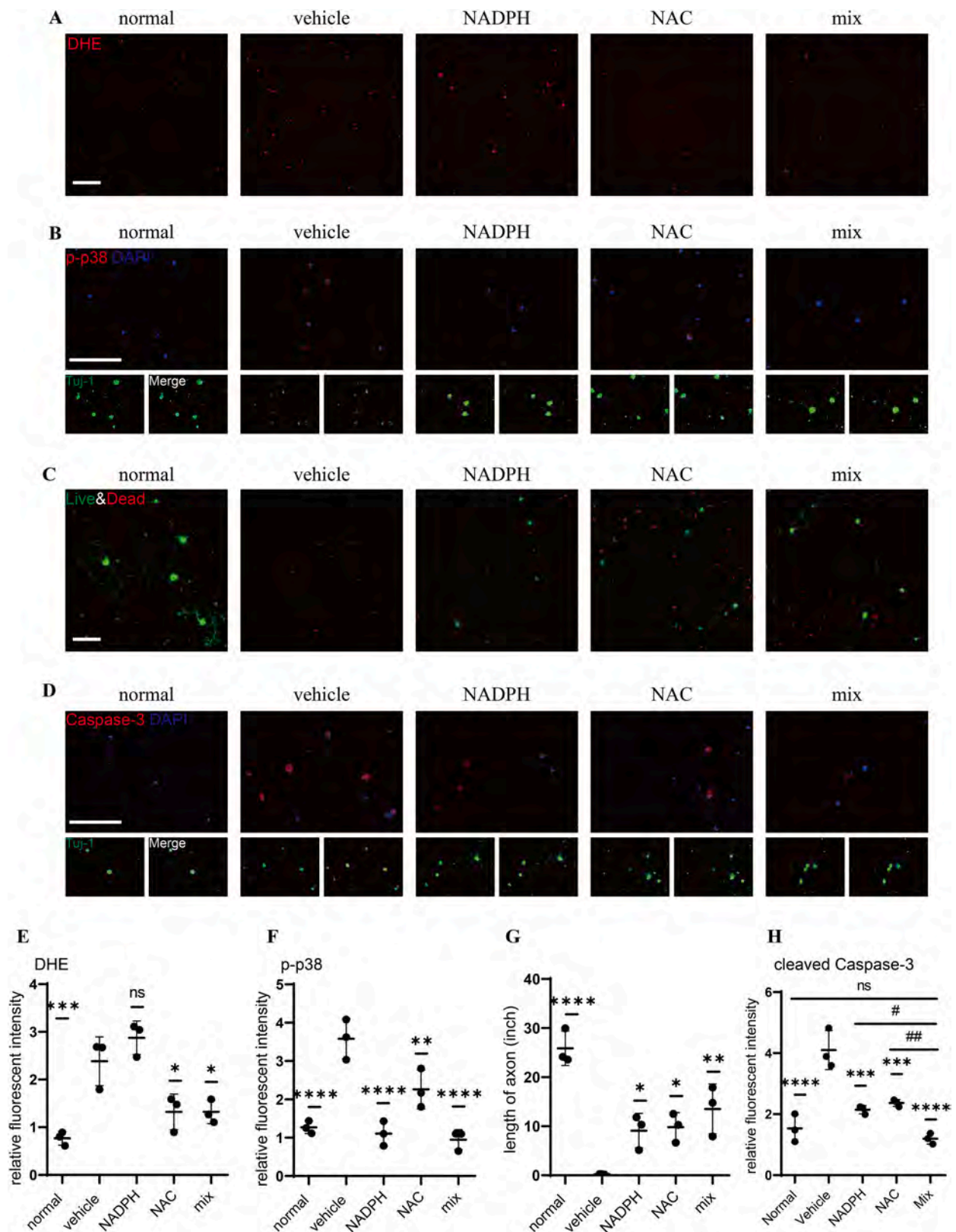
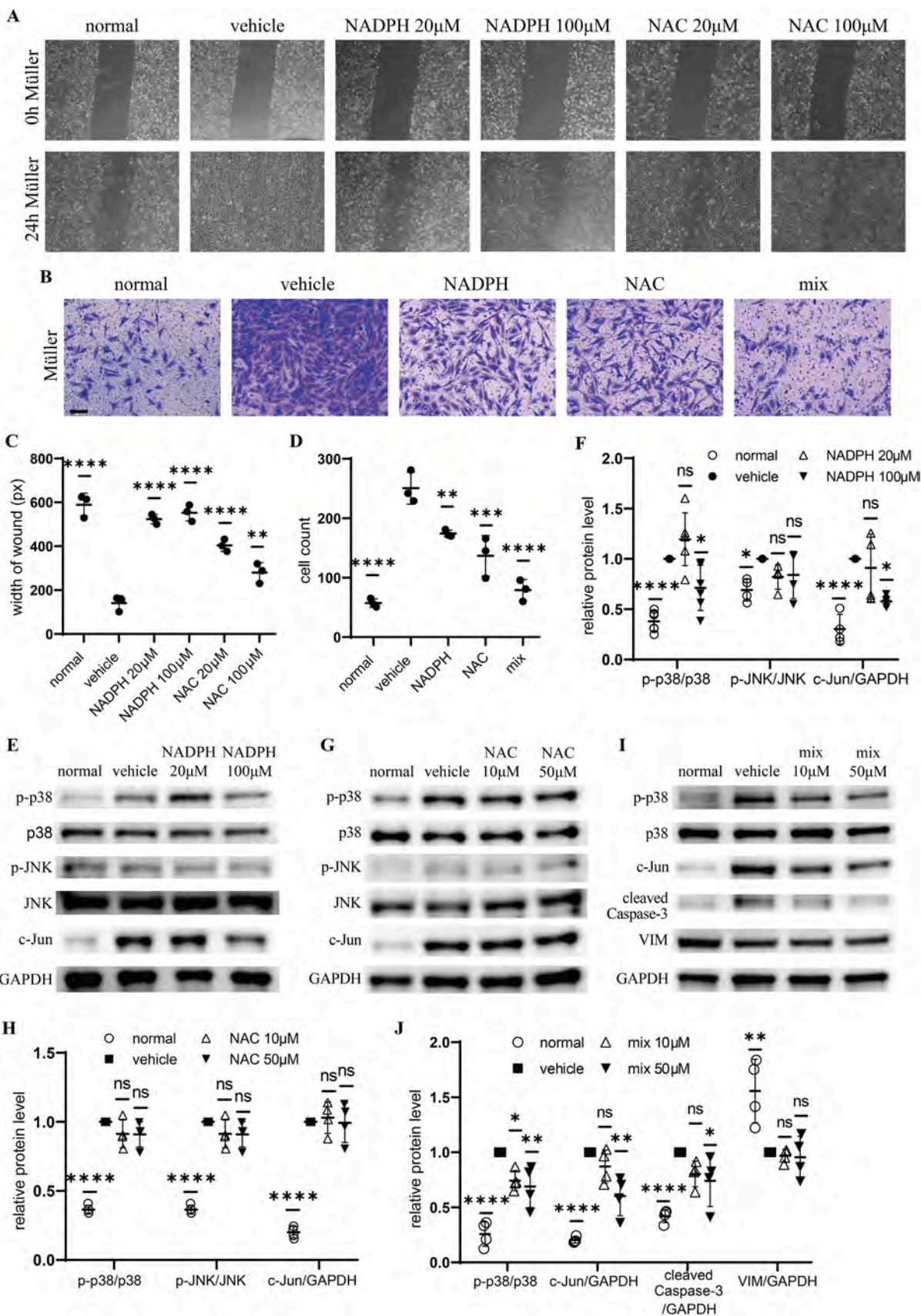


Fig. 3. Effects of NADPH/NAC on RGC intracellular ROS level and p38 activation after OGD. (A) Representative DHE staining images of normal primary RGCs and NADPH/NAC-treated OGD-injured RGCs and (E) statistics of DHE relative fluorescent intensity. (B) Representative p-p38 immunofluorescent images of normal primary RGCs and NADPH/NAC-treated OGD-injured RGCs and (F) statistics of p-p38 relative fluorescent intensity. (C) Representative live and dead cell staining of normal primary RGCs and NADPH/NAC-treated OGD-injured RGCs and (G) statistics of length of RGC axons. (D) Representative cleaved Caspase-3 immunofluorescent images of normal primary RGCs and NADPH/NAC-treated OGD-injured RGCs and (H) statistics of cleaved Caspase-3 relative fluorescent intensity. N = 3 per group. Error bars = SD. Scale bars = 100 μ m. Comparisons were conducted by one way ANOVA. ns = no significance. *: $p < 0.05$; **: $p < 0.01$; ***: $p < 0.001$; ****: $p < 0.0001$ compared with Vehicle group. #: $p < 0.05$; ##: $p < 0.01$ compared with Mix group.



(caption on next page)

Fig. 4. Effects of NADPH/NAC on Müller cell migration and p38/MAPK activation after OGD. (A) Representative scratch wound images from same location before and 24 h after OGD in normal and different concentrated NADPH/NAC treated Müller cells and (C) statistics of average width of each wound at 24 h after OGD. (B) Representative Transwell assay images of normal Müller cells and NADPH/NAC-treated OGD-injured Müller cells, cocultured with RGCs, and (D) statistics of migrated Müller cell number. (E) WB blots (numbers beside: molecular weight; unit: kDa) of MAPK pathway proteins from normal and different concentrated NADPH-treated OGD-injured Müller cells, and (F) statistics of their gray value. (G) WB blots (molecular weight: same as (E)) of MAPK pathway proteins from normal and different concentrated NAC-treated OGD-injured Müller cells, and (H) statistics of their gray value. (I) WB blots (numbers beside: molecular weight; unit: kDa) of p38/MAPK pathway and its downstream proteins from normal and different concentrated NADPH & NAC-treated OGD-injured Müller cells, and (J) statistics of their gray value. $n = 3$ or 4 per group. Error bars = SD. Scale bar = 100 μm . Comparisons were conducted by one way ANOVA. ns = no significance; *: $p < 0.05$; **: $p < 0.01$; ***: $p < 0.001$; ****: $p < 0.0001$.

varying degrees in other parts of the retina, involving the full layer. Cleaved Caspase-3 increased more slightly which may indicated a late, rather than early apoptosis. IHC of p-p38 in lesioned retinas showed high expression in the IPL and the outer plexiform layer (OPL) with a longitudinal striation-like localization, which was consistent with the localization of Müller cells in the corresponding samples, suggesting that p-p38 may be a key protein affecting both RGC loss and Müller cell gliosis.

3.2. Establishment of the chronic ocular hypertensive (COH) model in vivo and the OGD model in vitro

First, we modified the previously reported modeling method and constructed the COH model by AC injection of air-10 μm -6 μm -polystyrene microbeads distributed in PBS with 0.1 % carbomer (Fig. 2A). The retinal IOP of COH model rats increased significantly at 7 d, 14 d, 21 d, and 28 d, although a slow decrease was observed over time (Fig. 2B). The IOP in some individuals was not properly elevated at first, but an ideal level could be achieved after replicating injection 7 d later. Retinal paraffin sections of control and COH model rats were stained with H&E. In COH retinas, the number of cells in the RGCL decreased significantly to normal levels (Fig. 2C, D). In IF staining, Müller cells were activated along with RGC marker reduction in the both retinal and optic nerve sections from COH model rats (Fig. 2E, F). The WB images of total retinal protein showed that the levels of the neuronal marker NeuN decreased, while the levels of the Müller cell marker VIM markedly increased (Fig. 2G, H).

OGD was conducted in vitro to simulate COH injury in vivo. For OGD intervention of Müller cells, DMEM with 0.3 g/L glucose concentration and 5 % CO_2 and 0.5 % O_2 atmosphere were applied for 22 h. Even if OGD-reduced cell death was not taken into consideration (Figure S1A), OGD treatment significantly accelerated Müller cell gliosis, represented by a narrower wound than normal at 24 h (Fig. 2I, J) and obvious protrusions with high VIM expression (Figure S1B). For OGD intervention in RGCs, medium (formulated by RGC growth medium and glucose-free DMEM) with 0.3 g/L glucose concentration and a 5 % CO_2 and 0.5 % O_2 atmosphere was applied for 4 h. Live & Dead staining showed substantial cell death and loss of axons in the OGD group (Fig. 2K, L).

3.3. NADPH and NAC inhibited OGD-mediated ROS elevation and p38 activation, respectively, in RGCs

To explore the protective effect of NADPH and NAC against OGD, we treated RGCs with NADPH and NAC both separately and combined and analyzed the p38/MAPK pathway and ROS levels. RGCs were cocultured with Müller cells as mentioned in the Methods section.

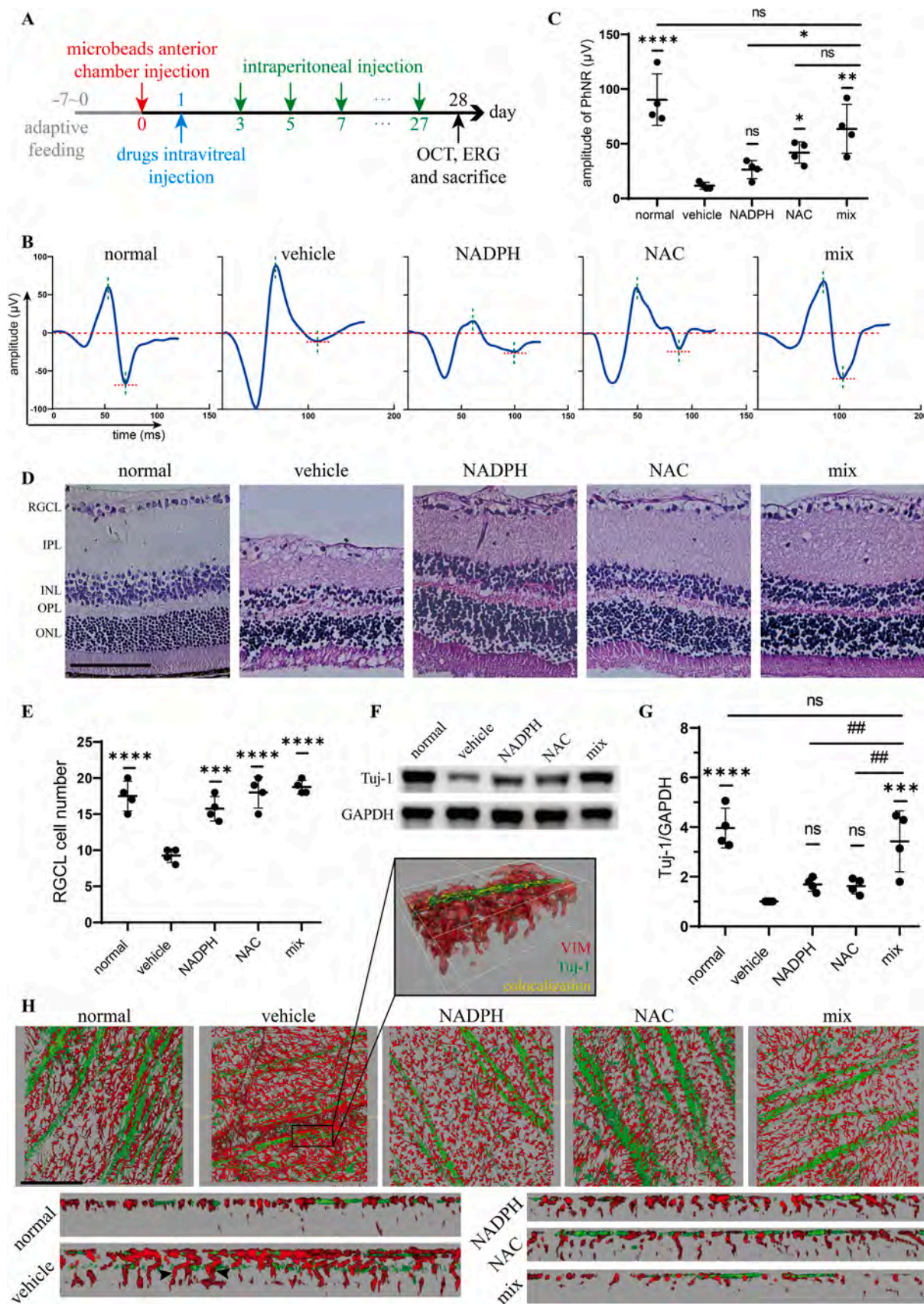
DHE staining showed a large increase in intracellular ROS levels after primary RGCs underwent OGD, and the addition of NAC almost completely inhibited the ROS level increase in the drug-treated group, while there was no statistically significant difference in the NADPH group. The mixture treatment showed similar results to those of the individual NAC treatment (Fig. 3A, E). After staining the cells with DHE, the cells were fixed and then exposed to light overnight, and p-p38 and β -tubulin III (Tuj-1) were stained. The results showed that OGD significantly upregulated p-p38 expression, and NADPH treatment inhibited the upregulation, while there was no significant difference in the NAC

group. The results of the combination treatment were similar to those of the individual NADPH treatment (Fig. 3B, F). The results of live and dead cell staining and costaining with ethidium homodimer-1 (EthD-1) and calcein acetoxymethyl ester (Calcein AM) showed that RGC death and axon disappearance were rescued by NADPH and NAC to varying degrees, and the combination treatment achieved a greater therapeutic effect (Fig. 3C, G). After live and dead cell staining and fixation, the cells were exposed to light overnight, and Caspase-3 and Tuj-1 expression were evaluated by IF. The images and quantitative analysis illustrated that OGD strongly upregulated the expression of Caspase-3, while NADPH and NAC inhibited the upregulation to varying degrees, and the mixture group showed a significantly greater effect than the two single-drug groups, decreasing the Caspase-3 fluorescence intensity close to the level of the control cells (Fig. 3D, H).

3.4. NADPH and NAC inhibited Müller cell migration via anti-ROS and anti-p38/MAPK mechanisms, respectively

We explored Müller cell horizontal and vertical migration through scratch wounding experiments and Transwell experiments, respectively. When Müller cells were cultured alone, horizontal migration after OGD was inhibited to varying degrees by different concentrations of NADPH or NAC, where 100 μM NADPH had the greatest effect, while NAC was more effective at 20 μM . Thus, we chose the optimal concentrations to use in the Transwell assay. The vertical migration of Müller cells after OGD increased, while NADPH and NAC reduced the migration of Müller cells to some extent, and the mixture group showed the greatest effect, close to the normal control (Fig. 4B, D). In addition, unlike OGD supernatants, reoxynogenated RGC supernatants had no effect on healthy Müller cells (Figs. S2A, 2B).

After extracting the total protein from Müller cells, we quantitatively analyzed the key proteins of the MAPK pathway. Since a high concentration of NAC had a limited inhibitory effect on proliferation during the scratch wounding experiments, we treated Müller cells with a lower concentration gradient for subsequent examinations. OGD-induced high expression of p-p38 in Müller cells was inhibited in the 100 μM NADPH group, while the p-p38 expression levels in the 20 μM NADPH group were not significantly different from those in the vehicle control group. Moreover, p-JNK levels were increased by OGD, and the effect of NADPH treatment was limited at all concentrations (Fig. 4E, F). In the NAC experiments, the expression levels of p-p38 and p-JNK were basically consistent between the OGD group and NAC groups, accompanied by no marked difference in the ratio with nonphosphorylated protein, and all of the OGD-treated samples had significantly higher levels than those in the control samples. This result suggested that NAC did not alter the activation of the p38/MAPK or JNK/MAPK pathways induced by OGD (Fig. 4G, H). We mixed NAC and NADPH and repeated the WB experiment. Interestingly, although low concentrations of NADPH or NAC alone showed little therapeutic effect, their combination downregulated the overexpression of p-p38 along with a stronger effect at high concentrations, leading to the inhibition of OGD-induced Caspase-3 upregulation. However, VIM levels remained stable among every treatment group and decreased after OGD treatment, which may be a result of a complicated in vivo environment and divergence between OGD and ocular hypertension. OGD was expected to promote the degeneration of the cytoskeleton.



(caption on next page)

Fig. 5. Protective effects of NADPH/NAC on COH-mediated neurodegeneration. (A) Time points of COH rats modeling, medication, measurements and sacrifice. (B) ERG curves of a healthy rat and NADPH/NAC-treated COH rats measured with PhNR program, and (C) statistics of PhNR amplitude (from PhNR wave trough to baseline). (D) Representative H&E staining images of healthy rats and NADPH/NAC-treated COH rats, and (E) RGCL cell number statistics. (F) WB blots (numbers beside: molecular weight; unit: kDa) of Tuj-1 from a healthy rat retina and NADPH/NAC-treated COH rat retinas, and (G) statistics of its gray value. (H) Representative surface rebuilt VIM & Tuj-1 immunofluorescent images of a healthy rat retinal mount and NADPH/NAC-treated COH rat retinal mounts. Square images showed vertical projections, the black rectangle showed a magnified stereo aspect, and the lowest 5 rectangle images showed horizontal projections of 5 μm -sections with arrow heads showing typical Müller cell gliosis. $n = 4$ per group. Error bars = SD. Scale bars = 100 μm . Comparisons were conducted by one way ANOVA. ns = no significance. *: $p < 0.05$; ***: $p < 0.001$; ****: $p < 0.0001$ compared with Vehicle group. ##: $p < 0.01$ compared with Mix group.

3.5. NADPH and NAC salvaged RGC function and number in COH model rats and Müller cell gliosis

In addition to in vitro experiments, we have also conducted pre- and post-dose studies in vivo to obtain results closer to the human body and provide a higher reference value for clinical practice.

After ensuring elevated IOP at Day 1, we used intravitreal (Day 1) and intraperitoneal injections (Days 3, 5, 7...27) for animal medication. At Day 28, we first conducted OCT and ERG examinations, and then the rats were sacrificed (Fig. 5A). Compared with control rats, the PhNR amplitude of COH model rats nearly dropped to baseline, while NADPH and NAC both rescued the amplitude of PhNR to different degrees, and the mixture group showed the greatest effect (Fig. 5B) with no significant difference between the combination and control groups (Fig. 5C), showing that the combination of the two drugs had a much greater effect than the individual components. We took OCT images of the retina and found that after modeling, the retinal thickness of the vehicle-controlled rats became significantly thinner and the retinal nerve fiber layer (RNFL) almost disappeared, but after treatment, the retinal thickness was partially restored, with RNFL thickening (Figure S3A). However, due to microbeads, the refracting media did not remain at an ideal clearance, so we were unable to perform statistical testing on the thickness information.

Thus, we further conducted H&E staining to analyze the cell number in the RNFL. Images showed that the number of RGCs was recovered in both the NADPH and NAC groups with significant differences, and the mixture group had a slightly higher number (Fig. 5D, E). The result paralleled the protein level of Tuj-1, showing a slight rebound in the single drug groups and nearly complete recovery in the mixture group (Fig. 5F, G). In addition, costaining of VIM and Tuj-1 in retinal mounts illustrated the morphological changes in Müller cells and RGCs. There was enhanced proliferation and distribution of Müller cells manifesting as dense and deep threading with RGC axon being invaded in COH model rats. Treatment with NADPH or NAC reduced the threading density of Müller cells (lateral projection) and partly restrained their activated shape with the recovery of nerve fibral integrity (horizontal projection). The mixture treatment reduced both threading density and depth, ameliorated Müller cell gliosis and better protected RGCs from damage (Fig. 5H).

3.6. NADPH and NAC inhibited RGC apoptosis via anti-peroxidation and anti-p38/MAPK mechanisms in vivo

We carried out corresponding mechanistic studies in vivo. The TEM images showed that RGCs of the control group had complete biomembrane structure, uniform nuclear membrane gap, loose chromatin, and oval or rod-shaped mitochondria with inner membrane sagging inward, forming plate-like cristae that were perpendicularly arranged along the long axis of mitochondria. In the vehicle group, nuclear chromatin was condensed into a half-moon or cap-like attachment to the nuclear membrane, and the mitochondria were swollen and enlarged with disorganized or lost cristae structure. In the NADPH group, condensed chromatin and disordered mitochondrial structure were partly recovered, and in the NAC group, nuclear membrane invagination was detected in addition to changes similar to those in the NADPH group. In the mixture treatment group, nuclear membrane invagination was shallower than that in the NAC group, and mitochondria were also

healthier (Fig. 6A). Similar mitochondria change and treatment-rescued demyelination were detected in optic nerves (Figure S3B). These results suggested that NADPH and NAC suppressed COH-mediated RGC apoptosis. In addition, we also counted the number of TUNEL-positive cells stained with the frozen sections. It was difficult to find TUNEL-positive cells in normal retinas, while a large number of TUNEL-positive cells appeared after COH and were mostly located in the RGCL, with only a small number of TUNEL-positive cells in the NADPH and NAC groups, which was significantly different. The combination treatment group showed a near-normal number of TUNEL-positive cells and retinal thickness (Fig. 6B, D). This result indicated that NADPH and NAC reduced the number of apoptotic RGCs under COH.

Finally, retinal ROS levels and the expression of core proteins in the p38/MAPK pathway were measured. DHE-stained frozen sections illustrated an outcome consistent to that in the in vitro experiment. ROS levels increased in COH retinas and were mainly eliminated by NAC and the mixture treatment, indicating that NAC played a more primary role than NADPH in ROS clearance (Fig. 6C, E). Blots of p38 and its downstream proteins were displayed and analyzed (Fig. 6F, G). Interestingly, both NADPH and NAC inhibited COH-mediated p38 phosphorylation enhancement, which was different from the in vitro results where NAC did not reduce p38 phosphorylation. IHC staining of p-p38 proved this result (Figure S3B). Effective molecules of p-p38, such as c-Jun, VIM and Caspase-3, also demonstrated synchronous changes, especially c-Jun and Caspase-3, which were significantly different, offering further therapeutic evidence for NADPH and NAC in COH-induced RGC injury and Müller cell gliosis. Noticeably, the combination treatment exerted greater effects than those of the components. A low dose of the mixture may result in the optimization of some inflammatory proteins, such as NLRP3, but some downstream or terminal markers, such as c-Jun or Iba-1, were only influenced by a high dose (Figure S3C, S3D).

4. Discussion

Glaucoma is the leading cause of irreversible blindness worldwide and is characterized by optic nerve degeneration [1], and the number of patients worldwide is projected to be 111.8 million in 2040 [29]. Exploring new safe and effective therapies for the treatment of glaucoma is now a popular research topic and the field is suffering from a bottleneck at present [30]. Although antioxidation methods have been used for decades, they are still inadequate. In this study, by establishing a novel COH rat model, we found that the mechanism of neurodegeneration and Müller cell gliosis in glaucomatous retinopathy may involve a common p38/MAPK pathway and peroxidation. NADPH and NAC, two small molecules that take part in the two intracellular antioxidant systems, and especially their combined use, relieved neurodegeneration by inhibiting p38/MAPK signaling and peroxidation, and neuroinflammation was also inhibited directly or through the relief of neuronal damage.

Oxidative stress is recognized as an important mechanism of cell death in many neurodegenerative diseases, including glaucoma [13]. RGCs consume oxygen at a 5-fold higher level than photoreceptors in the dark to maintain action potential and re-establishing resting potential; thus, RGCs demand plenty of mitochondria and are more sensitive to energy exhaustion [31]. Mitochondria are an important ROS source, and increasing evidence points suggests that there are other relevant sources of intracellular ROS, such as NADPH oxidases, cytochrome P450,

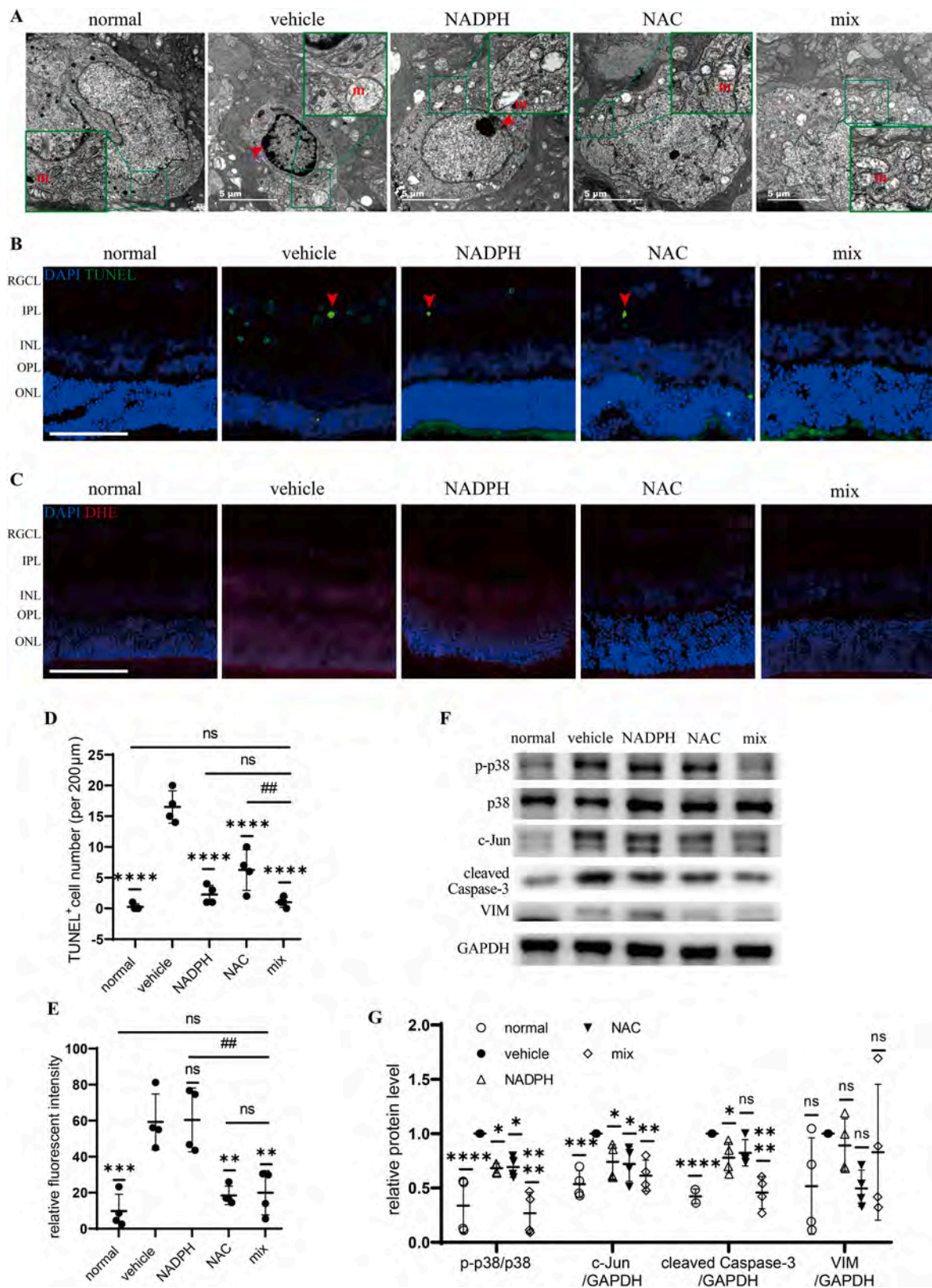


Fig. 6. Effects of NADPH/NAC on retinal ROS level, p38 activation and apoptosis after COH injury. (A) Representative TEM images of a healthy rat RGC and NADPH/NAC-treated COH rat RGCs. Green square showed higher magnification, arrow head indicated chromatin margination and letter “m” meant mitochondrion. Scale bar = 5 μm. (B) Representative TUNEL staining images of a healthy rat retina and NADPH/NAC-treated COH rat retinas, scale bar = 100 μm, and (D) statistics of TUNEL-positive cell number. (C) Representative DHE staining images of a healthy rat retina and NADPH/NAC-treated COH rat retinas, scale bar = 100 μm, and (E) statistics of DHE relative fluorescent intensity. (F) WB blots (numbers beside: molecular weight; unit: kDa) of p38/MAPK pathway and its downstream proteins from a healthy rat retina and NADPH/NAC-treated COH rat retinas, and (G) statistics of their gray value. n = 4 per group. Error bars = SD. Comparisons were conducted by one way ANOVA. ns = no significance. *: p < 0.05; ***: p < 0.001; ****: p < 0.0001 compared with Vehicle group. ##: p < 0.01 compared with Mix group.

lipoxygenases, and activated inflammatory glial cells during neuroinflammation [32]. Most studies have focused on RGC oxidative stress in glaucomatous neuropathy [33], but little attention has been given to Müller cell peroxidation, which may only reach a limited level in glaucoma due to the robust mitochondrial and glycolytic response of Müller cells under oxidative stress [34]. After discovering the occurrence of RGC apoptosis and Müller cell gliosis with p38 activation, we evaluated peroxidation in both RGCs and Müller cells under OGD, and found ROS level increases in the two types of cells and neuroprotective and anti-inflammatory effects after ROS inhibition. Peroxidation activates MAPK via oxidative modification of kinases in the MAPK pathway or promotional degradation and inactivation of MAPK phosphatase [35], and since the MAPK pathway is complexly involved in cell apoptosis, proliferation, stress and inflammation, it was investigated in RGCs and Müller cells [36]. The regulation of eukaryotic cellular redox status is provided by the glutathione and thioredoxin (TRX) systems, and the latter is a key endogenous antioxidative mechanism. Oxidation of cysteine thiols in TRX results in its dissociation from apoptosis signal-regulating kinase 1 (ASK1), triggering ASK1 autophosphorylation and downstream stimulation of p38 signaling [33], so we targeted these p38/MAPK molecules and found that p38 was involved in Müller cell gliosis. However, despite our detection of JNK/MAPK in Müller cells and the low sensitivity of Müller cells to OGD, NADPH and NAC, peroxidation and MAPK pathway signaling in different locations of glaucomatous retinas requires further research.

Substantial endeavors targeting genetics and epigenetics, microbiota, mitochondrial dysfunction and glial inflammation have been undertaken to elucidate the pathological mechanisms and to excavate underlying neuroprotective therapy of glaucoma [37]. In fact, manifold antioxidants have been investigated in various neurodegenerative diseases, including glaucoma. NAC was used to treat glaucoma model mice but demonstrated contradictory effects [21], while NADPH has been scarcely used in glaucoma studies. Here, we chose NADPH and NAC, intending to investigate the reduction reactions in the glutathione and TRX systems as well as their downstream signaling. Past neurodegenerative diseases studies have usually used NADPH or NAC individually and failed to obtain highly effective results. These results may be due to the independent relationship between glutathione and TRX systems; thus, their mutual compensation was limited. Coincidentally, NADPH and NAC played an inhibitory role in p38/MAPK signaling modification, which influences RGC apoptosis and glial inflammation. Some researchers have reported that glial cells have beneficial effects in glaucoma, such as activating the anti-inflammatory response [38], glutamate recycling [39], and neurotrophic factor biosynthesis [40,41], but long-term Müller cell gliosis is generally thought to be more harmful than protective [25]. We found that NADPH and NAC also targeted Müller cell peroxidation and p38/MAPK activation to prevent gliosis. What attracted us most was that NADPH, as a p38/MAPK inhibitor, and NAC, as an antioxidant, seemed to act independently *in vitro*, while their roles seemed to intersect *in vivo*. In addition, the time between the b wave and PhNR can reflect the function of electronic activities from photoreceptors to RGCs where Müller cells are located, and we discovered an elongation of the time under COH conditions and partial recovery after the combination (NADPH and NAC) treatment, however the explanation of this effect needs more consideration [28]. We have noticed that many studies on mechanisms in glaucomatous retinopathy paid attention to RGC damage itself and to Müller cells [41–43]. In summary, our study offers novel perspectives and clinical value on the roles of NADPH and NAC in relieving neurodegeneration and neuroinflammation by inhibiting peroxidation and p38/MAPK activation, which also provides a clinical approach to defend against other ischemic diseases. We believe that explicit interactions between these components in neuromodulation will be finally unfolded.

Ethics approval and informed consent statement

This study has been carried out in accordance with The Code of Ethics of the World Medical Association (Declaration of Helsinki) for experiments involving humans and followed the approval of the Human Research Ethics Committee of the Second Affiliated Hospital, Medical College of Zhejiang University (No. 120211118). Informed consent was obtained from all subjects involved in the study. All animal care and experiments were approved by the Laboratory Animal Ethics Committee of the Second Affiliated Hospital, Medical College of Zhejiang University (No.2023–004) and performed in accordance with the Association for Research in Vision and Ophthalmology Statement for the Use of Animals in Ophthalmic and Vision Research.

Funding statement

This work was supported by the National Natural Science Foundation of China (No. 82171045), the Key Program of the Natural Science Foundation of Zhejiang Province (No. LZ23H120001) and Zhejiang Provincial Public Welfare Technology Research Project (No. GF22H129113).

Author contribution statement

M.C. and K.W. conceived the project and designed the study; Z.L. supplied the design and fund support of experiments for revised manuscript; N.Y., C.Z. and X.W. performed the experiments and wrote the article; W.K and Q.Q. assisted for animal experiments and provided data analysis; Y.G., X.L. and Q.Z. supervised the study. All authors have reviewed and approved the final manuscript.

CRediT authorship contribution statement

Weishaer Ke: Investigation. **Xin Liu:** Funding acquisition. **Qi Zhang:** Supervision, Project administration. **Min Chen:** Supervision, Funding acquisition. **Xingdi Wu:** Investigation, Formal analysis. **Chengshou Zhang:** Validation, Investigation. **Qiyu Qin:** Methodology. **Yuxiang Gu:** Supervision. **Zhenjie Liu:** Conceptualization, Methodology. **Kaijun Wang:** Funding acquisition, Conceptualization. **Naiji Yu:** Writing – original draft, Investigation, Conceptualization.

Declaration of Competing Interest

The authors declare that they have no competing interests.

Data availability

All data generated or analyzed during this study are included in this published article and its supplementary information files and available from the corresponding authors on request.

Acknowledgements

We thank Beibei Wang and Yiping Lyu in the Center of Cryo-Electron Microscopy, Zhejiang University for her technical assistance with TEM.

We thank Di Wu in Zhejiang Provincial Key Laboratory of Ophthalmology for gifting MIO-M1 Müller cell line.

Appendix A. Supporting information

Supplementary data associated with this article can be found in the online version at [doi:10.1016/j.biopha.2024.116711](https://doi.org/10.1016/j.biopha.2024.116711).

References

- [1] H.A. Quigley, Glaucoma, *Lancet* (Lond., Engl.) 377 (9774) (2011) 1367–1377.
- [2] S. Tabak, S. Schreiber-Avissar, E. Beit-Yannai, Crosstalk between MicroRNA and oxidative stress in primary open-angle glaucoma, *Int. J. Mol. Sci.* 22 (5) (2021).
- [3] S.G. Jarrett, H. Lin, B.F. Godley, M.E. Boulton, Mitochondrial DNA damage and its potential role in retinal degeneration, *Prog. Retin. eye Res.* 27 (6) (2008) 596–607.
- [4] R.S. Sohal, S. Agarwal, M. Candas, M.J. Forster, H. Lal, Effect of age and caloric restriction on DNA oxidative damage in different tissues of C57BL/6 mice, *Mech. Ageing Dev.* 76 (2-3) (1994) 215–224.
- [5] N. Papaioannou, P.C. Tooten, A.M. van Ederen, J.R. Bohl, J. Rofina, T. Tsangaris, et al., Immunohistochemical investigation of the brain of aged dogs. I. Detection of neurofibrillary tangles and of 4-hydroxynonenol protein, an oxidative damage product, in senile plaques, *Amyloid* 8 (1) (2001) 11–21.
- [6] D.A. Butterfield, B.J. Howard, S. Yatin, K.L. Allen, J.M. Carney, Free radical oxidation of brain proteins in accelerated senescence and its modulation by N-tert-butyl-alpha-phenylnitronone, *Proc. Natl. Acad. Sci. USA* 94 (2) (1997) 674–678.
- [7] G. Fujino, T. Noguchi, K. Takeda, H. Ichijo, Thioredoxin and protein kinases in redox signaling, *Semin. Cancer Biol.* 16 (6) (2006) 427–435.
- [8] F. Tezel, Oxidative stress in glaucomatous neurodegeneration: mechanisms and consequences, *Prog. Retin. eye Res.* 25 (5) (2006) 490–513.
- [9] S. Pal, G.N. Rao, A. Pal, High glucose-induced ROS accumulation is a critical regulator of ERK1/2-Akt-tuberin-mTOR signalling in RGC-5 cells, *Life Sci.* 256 (2020) 117914.
- [10] B.J. Smith, C.F. McHugh, A.A. Hirano, N.C. Brecha, S. Barnes, Transient and sustained ganglion cell light responses are differentially modulated by intrinsically produced reactive oxygen species acting upon specific voltage-gated Na(+) channel isoforms, *J. Neurosci.: Off. J. Soc. Neurosci.* 43 (13) (2023) 2291–2304.
- [11] M. Guo, Y. Zhu, Y. Shi, X. Meng, X. Dong, H. Zhang, et al., Inhibition of ferroptosis promotes retina ganglion cell survival in experimental optic neuropathies, *Redox Biol.* 58 (2022) 102541.
- [12] P. Checa-Casalengua, C. Jiang, I. Bravo-Osuna, B.A. Tucker, I.T. Molina-Martínez, M.J. Young, et al., Retinal ganglion cells survival in a glaucoma model by GDNF/Vit E PLGA microspheres prepared according to a novel microencapsulation procedure, *J. Control. Release: Off. J. Control. Release Soc.* 156 (1) (2011) 92–100.
- [13] J.C. Fan Gaskin, M.H. Shah, E.C. Chan, Oxidative stress and the role of NADPH oxidase in glaucoma, *Antioxidants*(Basel) 10 (2) (2021).
- [14] J. Lu, A. Holmgren, The thioredoxin antioxidant system, *Free Radic. Biol. Med.* 66 (2014) 75–87.
- [15] I.S. Harris, A.E. Treloar, S. Inoue, M. Sasaki, C. Gorrini, K.C. Lee, et al., Glutathione and thioredoxin antioxidant pathways synergize to drive cancer initiation and progression, *Cancer Cell* 27 (2) (2015) 211–222.
- [16] M. Telorack, M. Meyer, I. Ingold, M. Conrad, W. Bloch, S. Werner, A Glutathione-Nrf2-thioredoxin cross-talk ensures keratinocyte survival and efficient wound repair, *PLoS Genet.* 12 (1) (2016) e1005800.
- [17] Tribble JR, A. Otmani, S. Sun, S.A. Ellis, G. Cimaglia, R. Vohra, et al., Nicotinamide provides neuroprotection in glaucoma by protecting against mitochondrial and metabolic dysfunction, *Redox Biol.* 43 (2021) 101988.
- [18] M. Liu, H. Li, R. Yang, D. Ji, X. Xia, GSK872 and necrostatin-1 protect retinal ganglion cells against necroptosis through inhibition of RIP1/RIP3/MLKL pathway in glutamate-induced retinal excitotoxic model of glaucoma, *J. Neuroinflamm.* 19 (1) (2022) 262.
- [19] P.K. Mandal, A. Seiler, T. Perisic, P. Kölle, A. Banjac Canak, H. Förster, et al., System x(c)- and thioredoxin reductase 1 cooperatively rescue glutathione deficiency, *J. Biol. Chem.* 285 (29) (2010) 22244–22253.
- [20] J. Zheng, M. Conrad, The Metabolic Underpinnings of Ferroptosis, *Cell Metab.* 32 (6) (2020) 920–937.
- [21] H. Sano, K. Namekata, A. Kimura, H. Shitara, X. Guo, C. Harada, et al., Differential effects of N-acetylcysteine on retinal degeneration in two mouse models of normal tension glaucoma, *Cell Death Dis.* 10 (2) (2019) 75.
- [22] A. Bringmann, A. Reichenbach, Role of Müller cells in retinal degenerations, *Front. Biosci.: a J. Virtual Libr.* 6 (E) (2001) 72–92.
- [23] A. Bringmann, I. Iandiev, T. Pannicke, A. Wurm, M. Hollborn, P. Wiedemann, et al., Cellular signaling and factors involved in Müller cell gliosis: neuroprotective and detrimental effects, *Prog. Retin. Eye Res.* 28 (6) (2009) 423–451.
- [24] Y. Miao, G.L. Zhao, S. Cheng, Z. Wang, X.L. Yang, Activation of retinal glial cells contributes to the degeneration of ganglion cells in experimental glaucoma, *Prog. Retin. Eye Res.* 93 (2023) 101169.
- [25] S.L. Roche, A.M. Ruiz-Lopez, J.N. Moloney, A.M. Byrne, T.G. Cotter, Microglial-induced Müller cell gliosis is attenuated by progesterone in a mouse model of retinitis pigmentosa, *Glia* 66 (2) (2018) 295–310.
- [26] G.A. Napper, M.J. Pianta, M. Kalloniatis, Reduced glutamate uptake by retinal glial cells under ischemic/hypoxic conditions, *Vis. Neurosci.* 16 (1) (1999) 149–158.
- [27] Q. Qin, N. Yu, Y. Gu, W. Ke, Q. Zhang, X. Liu, et al., Inhibiting multiple forms of cell death optimizes ganglion cells survival after retinal ischemia reperfusion injury, *Cell Death Dis.* 13 (5) (2022) 507.
- [28] L. Frishman, M. Sustar, J. Kremers, J.J. McNany, M. Sarossy, R. Tzekov, et al., ISCEV extended protocol for the photopic negative response (PhNR) of the full-field electroretinogram, *Doc. Ophthalmol. Adv. Ophthalmol.* 136 (3) (2018) 207–211.
- [29] Y.C. Tham, X. Li, T.Y. Wong, H.A. Quigley, T. Aung, C.Y. Cheng, Global prevalence of glaucoma and projections of glaucoma burden through 2040: a systematic review and meta-analysis, *Ophthalmology* 121 (11) (2014) 2081–2090.
- [30] X. Wu, K. Koniczka, X. Liu, M. Chen, K. Yao, K. Wang, et al., Role of ocular blood flow in normal tension glaucoma, *Adv. Ophthalmol. Pract. Res.* 2 (1) (2022) 100036.
- [31] J.J. Harris, D. Attwell, The energetics of CNS white matter, *J. Neurosci.: Off. J. Soc. Neurosci.* 32 (1) (2012) 356–371.
- [32] P.A. Dionísio, J.D. Amaral, C.M.P. Rodrigues, Oxidative stress and regulated cell death in Parkinson's disease, *Ageing Res. Rev.* 67 (2021) 101263.
- [33] M. Almasieh, A.M. Wilson, B. Morquette, J.L. Cueva Vargas, A. Di Polo, The molecular basis of retinal ganglion cell death in glaucoma, *Prog. Retin. eye Res.* 31 (2) (2012) 152–181.
- [34] S. Navneet, J. Zhao, J. Wang, B. Mysona, S. Barwick, N. Ammal Kaidery, et al., Hyperhomocysteinemia-induced death of retinal ganglion cells: The role of Müller glial cells and NRF2, *Redox Biol.* 24 (2019) 101199.
- [35] Y. Son, Y.K. Cheong, N.H. Kim, H.T. Chung, D.G. Kang, H.O. Pae, Mitogen-Activated Protein Kinases and Reactive Oxygen Species: How Can ROS Activate MAPK Pathways? *J. Signal Transduct.* 2011 (2011) 792639.
- [36] N. Trempelec, N. Dave-Coll, A.R. Nebreda, SnapShot: p38 MAPK signaling, *Cell* 152 (3) (2013) 656–e1.
- [37] F. Tezel, Molecular regulation of neuroinflammation in glaucoma: Current knowledge and the ongoing search for new treatment targets, *Prog. Retin. Eye Res.* 87 (2022) 100998.
- [38] Y. Yang, N. Wang, L. Xu, Y. Liu, L. Huang, M. Gu, et al., Aryl hydrocarbon receptor dependent anti-inflammation and neuroprotective effects of tryptophan metabolites on retinal ischemia/reperfusion injury, *Cell Death Dis.* 14 (2) (2023) 92.
- [39] A.M. López-Colomé, E. López, O.G. Mendez-Flores, A. Ortega, Glutamate receptor stimulation up-regulates glutamate uptake in human müller glia cells, *Neurochem. Res.* 41 (7) (2016) 1797–1805.
- [40] T. Harada, C. Harada, S. Kohsaka, E. Wada, K. Yoshida, S. Ohno, et al., Microglia-Müller glia cell interactions control neurotrophic factor production during light-induced retinal degeneration, *J. Neurosci.: Off. J. Soc. Neurosci.* 22 (21) (2002) 9228–9236.
- [41] H. Liu, K. Bell, A. Herrmann, S. Arnhold, K. Mercieca, F. Anders, et al., Crystallins play a crucial role in glaucoma and promote neuronal cell survival in an in vitro model through modulating müller cell secretion, *Invest. Ophthalmol. Vis. Sci.* 63 (8) (2022) 3.
- [42] S.H. Choi, K.Y. Kim, G.A. Perkins, S. Phan, G. Edwards, Y. Xia, et al., AIBP protects retinal ganglion cells against neuroinflammation and mitochondrial dysfunction in glaucomatous neurodegeneration, *Redox Biol.* 37 (2020) 101703.
- [43] Q. Li, Y. Cheng, S. Zhang, X. Sun, J. Wu, TRPV4-induced Müller cell gliosis and TNF- α elevation-mediated retinal ganglion cell apoptosis in glaucomatous rats via JAK2/STAT3/NF- κ B pathway, *J. Neuroinflamm.* 18 (1) (2021) 271.